Cell Reports
Physical Science

CellPress
OPEN ACCESS

Article

Photoinduced reversible phase transition in a phenothiazine-based metal-organic framework

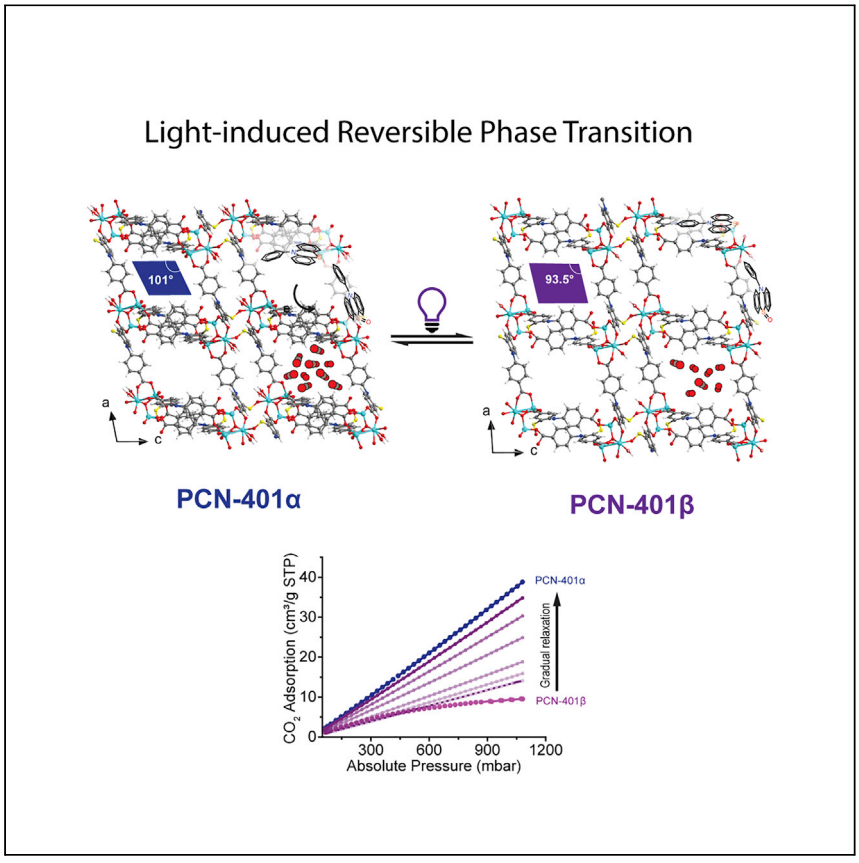

Xiao et al. report a photoresponsive MOF, PCN-401, which undergoes a structural change and radical formation upon light radiation. The photoresponsive behavior, caused by electron transfer among the phenothiazine-based ligands within the framework, brings about drastic property changes.

Zhifeng Xiao, Hannah F. Drake, Gregory S. Day, ..., Peiyu Cai, Matthew R. Ryder, Hong-Cai Zhou

rydermr@ornl.gov (M.R.R.)
zhou@chem.tamu.edu (H.-C.Z.)

Highlights

PCN-401 can go through a light-induced reversible phase transition

The oxygen content can tune the nucleation of PCN-401

The CO_2 adsorption changes drastically as it transitions between phases

Inter-ligand electron transfer under light was revealed as the mechanism

Xiao et al., Cell Reports Physical Science 3, 101074
October 19, 2022 © 2022
https://doi.org/10.1016/j.xcrp.2022.101074

Cell Reports
Physical Science

CellPress
OPEN ACCESS

Article

Photoinduced reversible phase transition in a phenothiazine-based metal-organic framework

Zhifeng Xiao,[1,5] Hannah F. Drake,[1,2,5] Gregory S. Day,[1,2] Jason E. Kuszynski,[1,3] Hengyu Lin,[1] Haomiao Xie,[1] Peiyu Cai,[1] Matthew R. Ryder,[2,*] and Hong-Cai Zhou[1,4,6,*]

SUMMARY

Photoinduced phase transitions in metal-organic frameworks are provoked by structural changes of photoresponsive linkers within the framework under light irradiation. These transitions are rare but fundamentally important as they can bring about light-switchability on a variety of properties of the materials. In this work, phenothiazine as a photoresponsive unit with distinctive photochemical properties is incorporated into a Zn-based metal-organic framework, PCN-401. The structural characterization of PCN-401 revealed a reversible structural transition upon light irradiation. The mechanisms behind the photoinduced phase transition are studied systematically by spectrometric methods and structural stability characterization. Our mechanistic studies successfully showcased how the phenothiazine unit in the framework undergoes structural transformation under light irradiation and how the reversible phase transition leads to the property changes. The findings have emphasized the significance of phenothiazine in photoresponsive materials and can serve as inspiration for the design and understandings of next-generation photoresponsive metal-organic materials.

INTRODUCTION

Photoresponsive metal-organic frameworks (MOFs) can undergo structural changes upon light irradiation, with many specific properties being photoswitchable. Switchable properties in MOFs have been reported that can influence the gas sorption, host-guest dynamics, mechanical properties, magnetism, and catalytic performance.[1–6] These photoresponsive MOFs are constructed by integrating photoactive motifs, including azobenzene, spiropyrans, anthracenes, stilbenes, and dithienylethenes into their porous structures.[1,3,4,7–22] The photoactive moieties can be introduced as guest molecules, pendant groups, or as framework scaffolds, which can offer an extremely versatile platform to study photoresponsive dynamics in a solid state.[1,3] When the moiety is incorporated into a framework scaffold, the photoresponsive motifs can bring about global structural changes on the framework under light irradiation, which can further render prominent changes in properties and enable photoswitchabilities.[23] However, such global structural changes are not always observed in MOFs with photoresponsive scaffolds due to the colossal constraints from the rigid framework. In rare cases in which photoinduced structural changes readily take place, the parent MOFs must have inherent structural flexibility from the cluster and/or the ligand.[24,25] MOFs with structural flexibility require achievable activation energies for this structural transformation.

[1]Department of Chemistry, Texas A&M University, College Station, TX 77843, USA

[2]Materials Science and Technology Division, Oak Ridge National Laboratory, Oak Ridge, TN 37831, USA

[3]Department of Chemistry & Biochemistry, Florida State University, Tallahassee, FL 32306, USA

[4]Department of Materials Science, Texas A&M University, College Station, TX 77843, USA

[5]These authors contributed equally

[6]Lead contact

*Correspondence: rydermr@ornl.gov (M.R.R.), zhou@chem.tamu.edu (H.-C.Z.)

https://doi.org/10.1016/j.xcrp.2022.101074

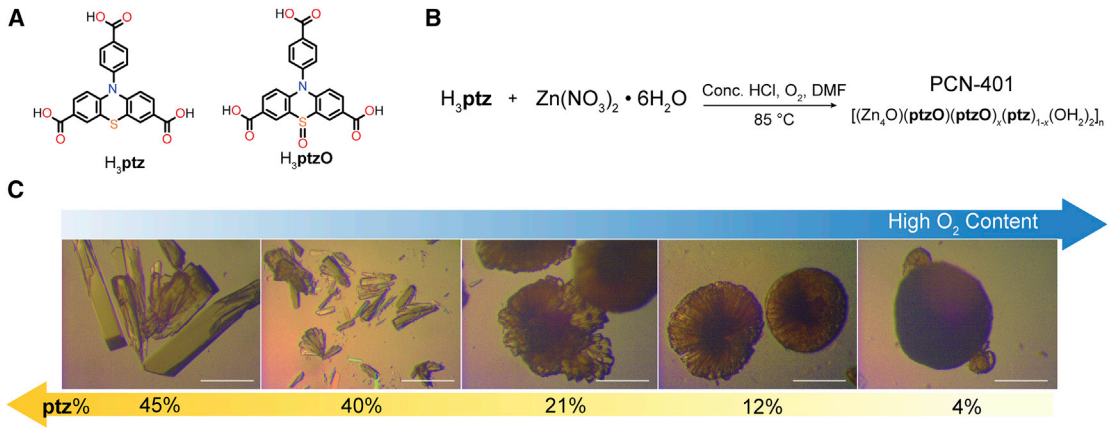

Figure 1. PCN-401 metal-organic frameworks (MOFs)

(A) H_3**ptz** and H_3**ptzO** linkers that comprise PCN-401.

(B) PCN-401 synthetic scheme.

(C) Images of the crystal morphologies with respect to the oxygen content of the DMF solution at synthesis and the corresponding **ptz** contents (**ptz**%) in the final MOF products (scale bar: 30 μm).

There has been a growing interest in expanding the potential properties of photoresponsive MOFs by expanding into less common photoresponsive motifs that have unique properties and promise fascinating potentials. Phenothiazine as a photoactive molecule has been extensively studied experimentally and computationally for its unique light-controllable isomerization and radical generation as well as for its biological activity.[26–30] In solution, the heteropolycyclic compound has been reported to undergo a reversible bent-to-flat isomerization and radical formation upon photoexcitation.[29,31,32] Such structural isomerization at the phenothiazine core usually stabilizes the photoinduced radicals and as a result produces a tremendous change in the molecular properties, particularly its magnetism, absorbances, and fluorescence. In the company of an electron acceptor, the structural isomerization becomes a redox event that can permanently alter the geometry of the phenothiazine core. In phenothiazine derivatives, the accessibility of the transition and its structural isomerization can be altered through geometric constraints of the photochromic unit.[33–35] In 2019, Kitagawa and coworkers reported a phenothiazine-based Cu MOF with unusual temperature-mediated pore-opening effects due to the structural flexibility dictated by the phenothiazine-based linker.[36] This important study showcased how the flexible phenothiazine ligand can be dynamically tuned by temperature and imposed global structural changes on the framework. We anticipated that the unique photochemical properties of the phenothiazine as well as its flexible nature would render unprecedented photoresponsivity in MOFs.

In this work, we investigated the photoresponsive effects of a phenothiazine MOF, PCN-401, that was assembled from Zn^{2+} and a new phenothiazine-based tritopic ligand, 10-(4-carboxyphenyl)-10H-phenothiazine-3,7-dicarboxylic acid, H_3**ptz** (Figure 1A). The photoinduced phase transition triggered by **ptz**-mediated intermolecular electron transfer in PCN-401 was systematically characterized and studied mechanistically to uncover the photoresponsive behavior of **ptz** in the framework.

RESULTS AND DISCUSSION

Synthetic studies of PCN-401

PCN-401 was synthesized by a 7-day solvothermal reaction of its ligand precursor, H_3**ptz**, and $Zn(NO_3)_2$ hexahydrate with hydrochloric acid as the modulator (Figure 1B).

In our initial synthetic studies, the as-synthesized PCN-401 crystals were digested in D_2SO_4 to investigate the ligand concentrations with ^1H NMR and mass spectrometry (Figures S6–S9). Unexpectedly, the NMR spectra and mass spectra of the digested MOF revealed that the starting ligand, H_3**ptz**, was partially oxidized into its oxide,10-(4-carboxyphenyl)-10H-phenothiazine-3,7-dicarboxylic acid 5-oxide (H_3**ptzO**), which implied an *in situ* oxidation event during the synthesis of PCN-401 (Figure 1A). As found in a series of systematic synthetic studies, using DMF with higher dissolved O_2 content resulted in a faster crystallization, a higher tendency toward polycrystal formation, and a higher average **ptzO** content in the resultant PCN-401 (Figure 1C) as determined by MOF digestion and ^1H NMR studies (experimental details in the supplemental information). These findings implied that the rate of H_3**ptz** oxidation has a great influence on the nucleation and growth of the PCN-401 crystals as higher oxygen content was expected to promote the **ptz** oxidation into **ptzO** during MOF formation. It has been previously reported that oxygen can serve as a mediated synthetic condition for solvothermal synthesis, but to our knowledge, this process is rare in supramolecular chemistry.[37] An effort to eliminate the oxidation entirely by using fully deoxygenated DMF under an inert atmosphere still resulted in 55% **ptzO** in the as-synthesized MOF, which implied that the starting ligand, H_3**ptz**, can also be oxidized by the HNO_3 produced from $Zn(NO_3)_2$ and HCl in the synthesis. This conclusion was further confirmed by the fact that replacing the Zn salt or acid modulator did not yield the same MOF. The unique behavior of PCN-401 crystallization under different O_2 concentrations gave us the tool to tune the **ptz**:**ptzO** ratio in the framework that has proven to be important in the photoswitchability of PCN-401. PCN-401 and the **ptz** and **ptzO** ligands were fully characterized (Figures S3–S6).

Structural characterization

Single crystal X-ray diffraction (SCXRD) studies were used for structural determination. Analysis indicated that PCN-401 crystallizes into a centrosymmetric space group, *C*2/*m*, regardless of the **ptzO** content. In the structure, a disordered Zn_4O-based cluster is formed, connecting 7 ligands and forming a 3-dimensional (3D) non-interpenetrated network. The metal cluster adapts a mirror symmetry with 2 groups of Zn^{2+} ions and connecting 7 ligands via carboxylate and sulfoxide donors (Figure 2A). The first group of Zn^{2+} ions reside inside the mirror plane and adopt a tetrahedral geometry, while the second group of Zn^{2+} ions is generated by the mirror plane and adopts the same geometry due to symmetry restrictions. After deconvoluting the disorder by removing the mirror symmetry, it can be seen that the two Zn^{2+} ions adopt two coordination geometries, distorted octahedron and tetragonal pyramid, with 1 coordinating water molecule on each side. There are 2 crystallographically distinctive ligands connecting the metal clusters (Figure 2A). The first kind, called L_A, connects 4 clusters with 3 carboxylate groups and 1 sulfoxide group. The sulfoxide group in L_A bridges 2 Zn ions with 2 Zn-O bonds of 2.25 Å, which are longer than the usual sulfoxide O-Zn bond found in the structure database. Such bridging coordination mode from the sulfoxide is quite rare in coordination chemistry, however. We expect that based on the cluster structure of PCN-401, the bridging coordination bond is essential to the formation and integrity of the cluster. Therefore, the L_A must be **ptzO**, which indicates that the *in situ* oxidation during the solvothermal reaction is critical to the cluster and structure formation. The phenylcarboxylate group on L_A is disordered by the ***ac*** mirror plane as one of the carboxylate oxygen atoms and is shared by 2 Zn^{2+}. The second kind, L_B, connects 3 clusters with 3 carboxylate groups and thus can be either **ptzO** or **ptz**. In the refined structure, L_B exhibits 2-fold position disordering, particularly on the coordination mode of the phenylcarboxylate group. We assumed that such disordering was caused by the different configurations of **ptz** and **ptzO** that are concurrent at the L_B site. The

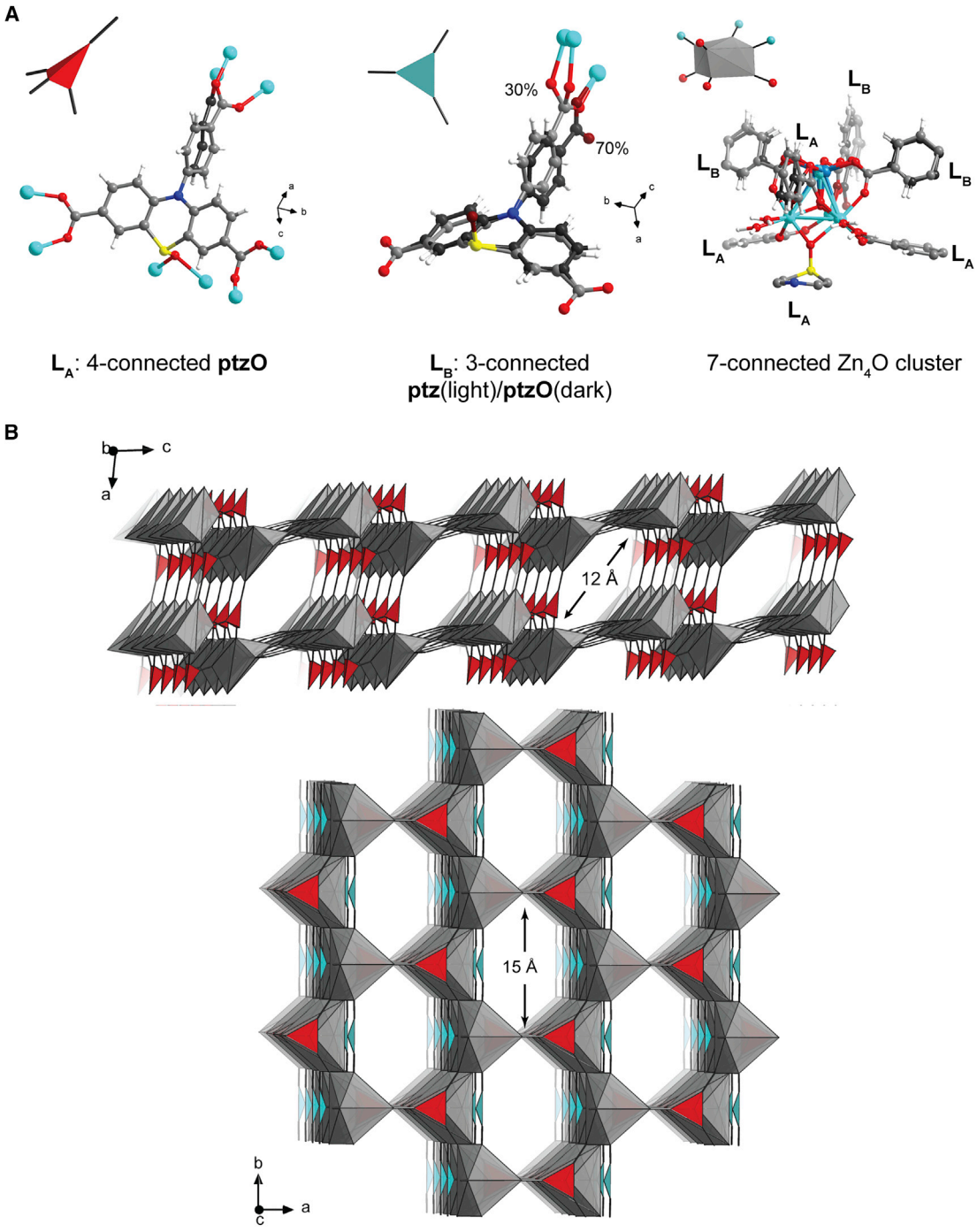

Figure 2. Metal-organic framework structure

(A) Structures of **ptz**/**ptzO** linkers and cluster in PCN-401.

(B) Topological schemes of PCN-401 structure on ***ac*** and ***ab*** planes showing the pore sizes.

phenylcarboxylate in the **ptzO** part of L_B was refined to a monodentate coordination mode with a 70% occupancy, while that in the **ptz** part was refined to a bridging coordination mode. The refinement results showed that the crystal mounted had a **ptz** content of 15%, which was unexpectedly low for a large single crystal. This discrepancy implied that the **ptz** ligand can partially adapt to the **ptzO** configuration in the

L_B site, which led to an underestimated occupancy of the **ptz** ligand upon refinement. This implication was further supported by the fact that the extra Zn-O bond in the **ptz** part has a bond length of 2.250(3) Å, outside the range of a normal Zn-O coordination bond, indicating that the extra bonding for the **ptz** part did not significantly contribute toward the cluster formation. The strength of such interactions may not offer enough stabilization toward an exclusive binding mode for **ptz**. Moreover, the unique coordination modes and disordering exhibited in the refined structure implies a high degree of flexibility that makes it potentially susceptible toward structural isomerization. Topologically, the Zn_4O-based cluster is considered a 7-connected node. The **ptzO** ligands serve as 4-connected nodes (L_A) and 3-connected nodes (L_B) (Figure 2B). The connections between the metal cluster and ligands results in an infinite 3D (3, 4, 7)-connected 3-nodal net, which represents a new topology as analyzed by the ToposPro program.[38] The new topology is called the **xdz** topology as it would appear in the MOF topology databases. In the packed structure, the L_A ligands pair up in an antiparallel manner to form a pillar structure along the ***a*** direction. In the ***b*** direction, the clusters pack along a 2_1-screw axis and are chained by the staggered L_A disordered ligands. The arrangement of the ligands in the structure results in two relatively large pore channels in the microporous scale along the ***b*** and ***c*** directions, respectively (Figure 2B).

To characterize the pore structures of PCN-401, the activated PCN-401 samples were subjected to gas adsorption Brunauer-Emmett-Teller (BET) studies. It is noteworthy that PCN-401 can be activated only through supercritical CO_2 exchange[39] but not with conventional thermal activation under vacuum potentially due to the framework collapse during the thermal activation, which is commonly seen in flexible MOFs.[40] After activation, the N_2 isotherms at 77 K indicated that the structure is microporous with a surface area of 3,500 m^2/g (Figure S16B). The type I isotherm shape of the adsorption indicated that the framework is microporous.[41] The pore size distributions were calculated via density functional theory (DFT) methods and matched well with the single crystal experimental determination (Figure S16A). Additional gas sorption studies for PCN-401 toward CH_4 and CO_2 may be found in Figure S17 and Tables S2–S4.

Light-induced reversible phase transition

Under irradiation by 365 nm light, PCN-401 exhibits fast photochromism accompanied by the disappearance of fluorescence. The photochromism was later characterized by solid-state UV-visible spectrometry, indicating that 2 peaks arose at 548 nm and ~800 nm, respectively, after UV irradiation (Figure 3A). It has previously been reported that the light absorbance change can be attributed to the radical formation and conformation change in phenothiazine.[33] To capture the fast photochromism event, we exploited the fluorescence decay of the process using fluorescence microscopy (Figure S12). As shown in Figure 3B, 50% reduction of the fluorescence took place in the first 10 s under 100% light intensity, which could be a sign of a fast synergistic process in the crystal lattice. We initially suspected such an effect was caused by aerobic oxidation of the ligand under light. To verify the assumption, we compared the **ptz**:**ptz**O ratio before and after UV irradiation by ^1H NMR spectra of the digested MOF samples and found that the ratio was not changed by UV irradiation, which proved the process did not involve aerobic oxidation. Moreover, the photochromism was later found to be reversible at room temperature. Two days after the UV irradiation, the color and fluorescence were recovered as evidenced by the solid-state UV-visible spectrum (Figure 3A) and fluorescence microscopy studies (Figure S13B). To better understand the photoresponsiveness, we conducted gas sorption studies on the UV-irradiated activated samples. To our surprise, the

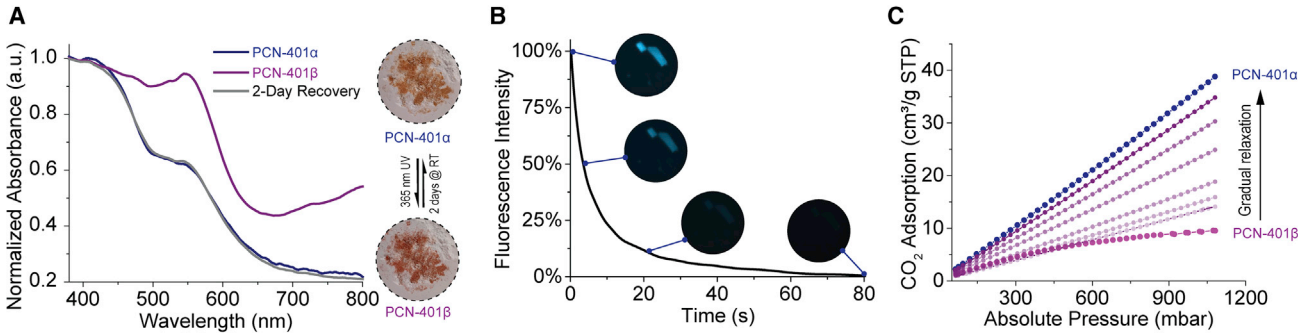

Figure 3. Photochemical properties and phase transition

(A) Photochromism of PCN-401 under UV irradiation.

(B) Fluorescence decay of PCN-401 during phase transition.

(C) CO_2 isotherms of PCN-401 at 273 K showing the change during the relaxation of β phase into α phase in the 96 h after the phase transition.

CO_2 sorption of the framework at room temperature was reduced by 75% at 1 bar after light irradiation (Figures 3C and S20). The CO_2 sorption reduction upon UV irradiation can be categorized as the light-induced switchable adsorption (LISA) effect.[3,12,42] Such an effect may be an indication that structural transitions have taken place during light irradiation, causing a shift in the host-guest interactions. The fact that the N_2 isotherm and surface area of the post-irradiated sample remained unaltered by the transition implies that the porous nature of the MOF remains intact after UV irradiation (Figure S19). Like the photochromism, the recovery of CO_2 sorption behavior was observed within 2 days. The gradual relaxation of the framework after the isomerization was clearly observed by the CO_2 sorption at serial time points after UV irradiation. We therefore concluded that UV can induce reversible phase transition on PCN-401. The as-synthesized phase was denoted as PCN-401α and the phase obtained by UV irradiation was called PCN-401β.

Under light irradiation, phenothiazine and its derivatives are strong electron donors and capable of transferring an electron to an appropriate acceptor in proximity to it.[26–28,43,44] Such a photoinduced charge separation event can induce radical formation and molecular configuration change in the solution.[27,45] We suspected that the phase transition was caused by the light-induced isomerization of phenothiazine cores within the framework. To directly observe the structural changes brought about by the phase transition, single crystals of PCN-401β were obtained by extended UV irradiation of PCN-401α and characterized by SCXRD. Despite our effort to retain the crystallinity during UV irradiation, most of the PCN-401α crystals disintegrated and lost birefringence. Fortunately, we were able to obtain 1 dataset with sufficient quality that helped us to understand the structural change. From the diffraction pattern, PCN-401β crystallized into the same crystal lattice type, *C*-centered monoclinic. When it comes to the unit cell parameters, the axis length differences are <3%, while the **β** angle changed from 100.889(2)° in the α phase to 93.38(4)° in the β phase (Table S1). After integration, the R_{int} value of the dataset was 13.1%, with a 98% completeness, presumably due to the slow deterioration of the crystal during the measurement. In the refined structural model of PCN-401β, the ligand configurations exhibit different degrees of variability compared to those found in PCN-401α (Figure S15). In L_A, the interplanar angle between the *N*-phenyl plane and the phenothiazine plane decreased from 162.2(1)° in the α phase to 154(1)° in the β phase (Figure S15A). While in L_B, the position disordering resulted from concurrency of **ptz**, and **ptzO** was not observed from the electronic map, potentially due to the poor resolution of the

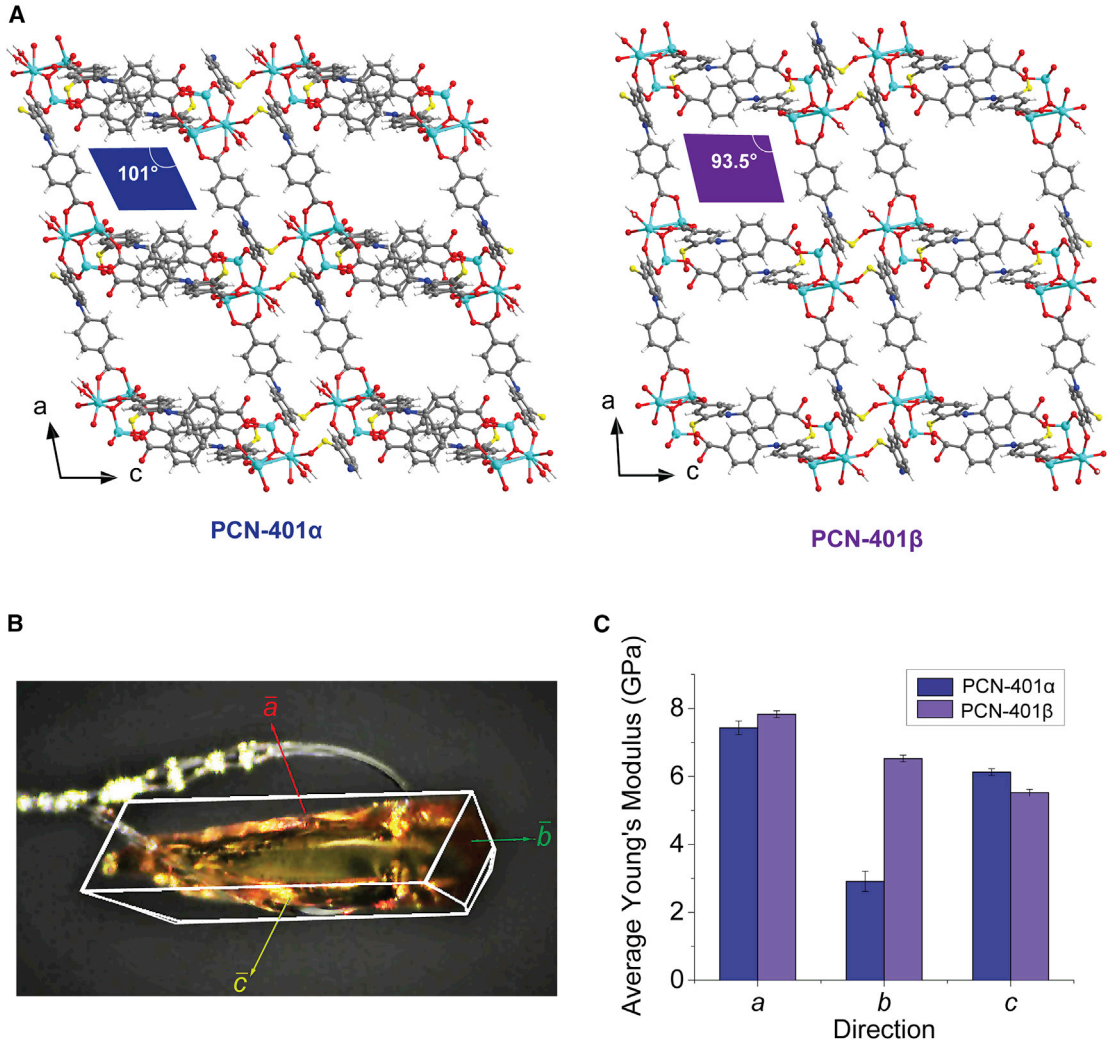

Figure 4. Structural effect of phrase transition

(A) Crystal structures of PCN-401 α and β showing the differences in the pore shape after phase transition.

(B) Crystal indexing of PCN-401.

(C) Young's moduli of PCN-401α and β.

dataset. The phenyl configuration change of L_B was found to be very minor (<1° difference with uncertainty) (Figure S15C). Interestingly, in both L_A and L_B, the phenothiazine ring became less flat by 1.47(2)° in L_A and by 4.2(9)° in L_B (Figures S15B and S15D), which was the opposite of our initial assumption made based on how phenothiazine and its derivatives reportedly behave in solution. As for the cluster, elongation on the sulfoxide O-Zn coordination bonds was observed in the β phase compared to that in the α phase. The change in the coordination bond was an adjustment from the ligand configuration change during the phase transition. As found in the packed structure (Figure 4A), the pore window in the *ac* plane morphed toward a more rectangular shape. The void percentage in the α phase was calculated to be 52% with the Platon program package,[46] while that in the β phase was 57%, potentially due to the change in pore shape. Despite the poor quality of the dataset, the observations in the ligand configuration and pore shape in the β phase are convincing as these structural differences are too significant to be accounted for by model errors.

Mechanical properties

Phase transitions in crystalline materials are often accompanied by mechanical property changes.[47,48] In these materials, the molecular configuration shifts in the microscopic scale and are ordered and uniform. These changes can accumulate and magnify into prominent change in the macroscopic scale. In the case of the light-induced phase transition in PCN-401, we assumed the global structural changes could be manifested by anisotropic changes in the hardness and elasticity of the single crystals. To characterize the anisotropic mechanical properties and correlate the change with the crystal structures, crystal face indexing of the single crystals of PCN-401 were carried out on a diffractometer. Conveniently, the block-shaped crystals of PCN-401 exposed ($\bar{1}$ 00), (0$\bar{1}$ 0), and (00$\bar{1}$) faces that can be studied by nanoindentation (Figures 4B and S21). The Young's modulus of a material, a measure of how easily the material can deform, can be determined through nanoindentation experiments on single crystals of the PCN-401. Several large single crystals were mounted in epoxy resin, exposing a clean crystallographic plane of the single crystal, with several crystals oriented to expose all 3 indexed faces on several single crystals. After determining the Young's moduli of the PCN-401α samples, the samples were irradiated by UV *in situ* to induce the α-to-β phase transition. The Young's moduli were then determined on β phase samples on the same crystals that were measured previously in the PCN-401α phase. Each sample was calculated in quadruplet with a 20-nm change in position on the clean crystal surface. The results are shown in Figures 4C and S22. The results indicate the PCN-401α went through anisotropic stiffening as it transitioned to the β phase. The Young's modulus along the ***b*** axis in the β phase is 2 times that in the α phase, while the Young's moduli along the ***a*** and ***c*** axes are within statistical variance between the 2 phases. The abrupt and prominent anisotropic stiffening further confirmed that the phase transition in PCN-401 is not domain bound in the 3D lattice but global and uniform. From the crystal structures of PCN-401, the phenothiazine planes of the 2 kinds of ligands, L_A and L_B, are aligned along the ***b*** axis (Figure S14). As the α phase transitions to the β phase under light, these planes deviate more from the flat configuration, which can contribute to the stiffening effect along the ***b*** axis. This kind of mechanical response in PCN-401 to the light is rare in photoresponsive MOFs. These results are consistent with what has been observed in mechanical property studies in MOFs,[49–51] but to our knowledge this is the first report of this phenomenon in a phenothiazine-based framework.

Mechanistic studies of the photoinduced phase transition

We hypothesized that the phase transition is likely caused by the unique photoresponsive behavior of **ptz** in the framework, and therefore the **ptz** content in the framework is expected to be crucial to the photoresponsivity and the property changes associated with the phase transition. As previously mentioned, the synthetic studies showed that the **ptz**/**ptzO** content in as-synthesized PCN-401 can be tuned by O_2 concentration in the DMF. To identify the influences of **ptz** content on the photoresponsive behavior, a sample with high average **ptz** content (20%), called **h**-PCN-401, and a sample with low average **ptz** content (8%), called **l**-PCN-401, were characterized and compared in the following studies. Initially, the **l**- and **h**-PCN-401 samples were compared in the photochromism studies, wherein the absorbances of the samples were compared before and after photoinduced transition. As shown in Figures S11A and S11B, the spectra of both samples exhibit 2 newly arisen peaks at 548 nm and ~800 nm, respectively. Specifically, the peak at 548 nm in the **h**-PCN-401 spectrum increases by 75%, a much higher increase compared to the 32% increase in **l**-PCN-401. After the transition, the relaxation kinetics of β phase to α phase in these 2 samples were monitored at room temperature using the

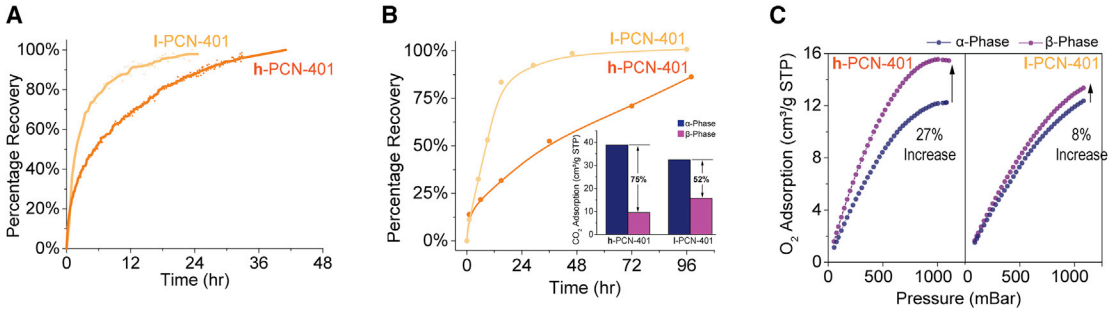

Figure 5. Relaxation kinetics

(A and B) Relaxation kinetics of α-to-β phase in PCN-401 tracked by (A) the absorbance at 548 nm; (B) CO_2 adsorption at 273 K and 1 bar; inset in (B) shows the CO_2 adsorption changes upon phase transition at room temperature and 1 bar.

(C) O_2 isotherms of PCN-401 at 195 K.

548-nm peak. The results indicated that under room temperature, the relaxation in **l**-PCN-401 took ~1 day, while that in **h**-PCN-401 took >2 days (Figure 5A). These differences implied that a higher unoxidized **ptz** content in PCN-401 can lead to a more accessible and stable β phase, which leads to higher activation energy for the β-to-α transition. The stability disparity between **h**- and **l**-PCN-401 was further proven by the CO_2 adsorption recovery after UV irradiation, where **h**-PCN-401 exhibited a slower recovery than **l**-PCN-401 (Figure 5B). Interestingly, **l**-PCN-401α adsorbed slightly less CO_2 at 1 bar than **h**-PCN-401β, while the N_2 adsorption and pore sizes remained the same. When transitioning to the β phase, **l**-PCN-401 exhibited a LISA effect of a 52% reduction in CO_2 adsorption compared to the 75% decrease in that seen in **h**-PCN-401. To our knowledge, such a tunable CO_2 LISA effect based on ligand content in the same MOF is unprecedented in photoresponsive MOFs. These findings also indicated that **ptz** interacts more strongly with CO_2 than **ptzO** in the framework. Hypothetically, the phase transition has altered the electronic structure[33,44,45] of the **ptz** that results in an outstanding decrease in CO_2 interactions. This hypothesis was furthered verified by O_2 adsorption studies of different PCN-401 phases. Unlike CO_2, the O_2 isotherms of **l** and **h**-PCN-401α are the same within experimental error (Figure 5C). But in the β phase, the O_2 uptake at 1 bar and 195K of **h**-PCN-401β increases by 27% while that of **l**-PCN-401β increases by 8% (Figure 5C). The heat of adsorption toward O_2 (HOA_{O2}) was calculated using reported methods[52–55] and is also consistent with the difference. The HOA_{O2} of **h**-PCN-401 at 0.4 cm^3/g uptake increases by 3 kJ/mol and that of **l**-PCN-401 increases by only 1 kJ/mol upon the α-to-β transition (Figure S18). The enhanced interaction with O_2, a paramagnetic gas, after transitioning to the β phase could be an indirect indication of radical formation upon light irradiation. In the meantime, the drastic decrease in CO_2 adsorption and increase in O_2 adsorption result in a 2.3 times increase in O_2/CO_2 selectivity for **h**-PCN-401 upon the α-to-β transition. This kind of light-induced gas selectivity change phenomenon in MOFs was recently described by Guo and coworkers for the first time,[56] in which a photoinduced electron transfer (PIET) event was proposed to be the cause of the CO_2/C_2H_2 selectivity change in the MOF. The example shown in this work further proves the universality of the gas selectivity switching strategy.

To further confirm the existence of radicals in the β phase, we conducted electron paramagnetic resonance spectroscopy (EPR) experiments on both the **l**- and **h**-PCN-401 samples at 4 K. The results indicated that only upon transitioning to the β phase after light irradiation did the EPR signals start to appear in both **l**- and **h**-PCN-401 samples (Figure 6A). Although solid-state EPR cannot reliably be

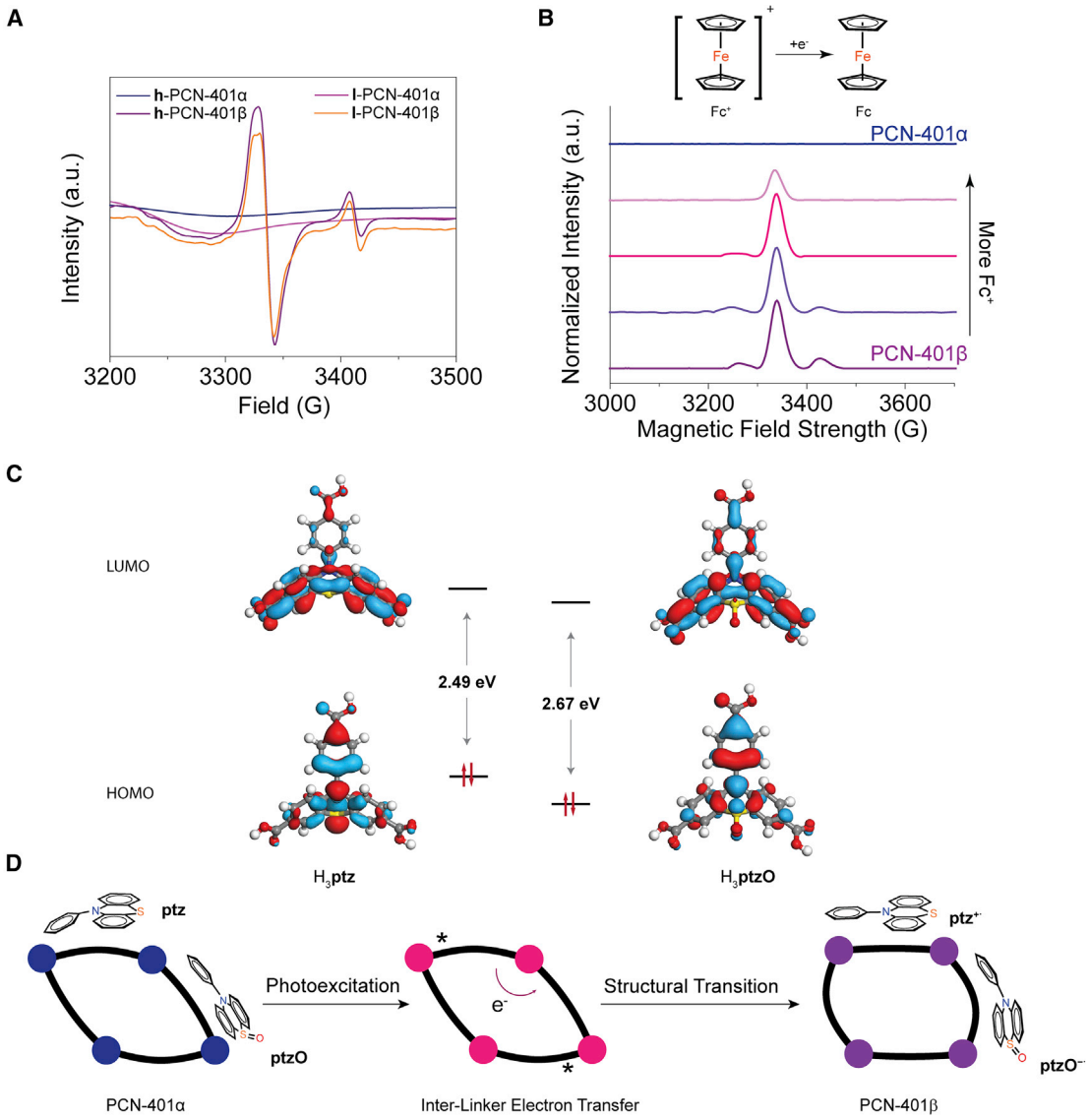

Figure 6. Phase transition mechanism

(A) The EPR spectra of PCN-401 of different phases and **ptz** contents at 4 K.

(B) EPR spectra at 4 K showing the extinction of different radicals during the titration Fc^+ into the PCN-401β.

(C) Computed HOMO and LUMO energy profiles of H_3**ptz** and H_3**ptzO**.

(D) Proposed photoinduced electron transfer mechanisms behind the phase transition.

interpreted in a quantitative manner, stronger signals observed in **h**-PCN-401 than in **l**-PCN-401 under the same experimental conditions can still be indicative of a higher radical concentration in **h**-PCN-401. The fact that the degrees of photochromism and the CO_2/O_2 adsorption change upon phase transition are positively correlated with the **ptz** content in the samples implies that the radical formation does not originate from the **ptzO** but from **ptz** in the framework.

A recent study shows that the PIET behavior of phenothiazine derivatives shifts as they are oxidized into sulfoxide or sulfone.[33,44,45,57] In PCN-401, the coexistence of **ptz** and **ptzO** can be crucial in forming a route of electron transfer. Hypothetically, the radical observed in the β phase results from the photoexcited electron hopping

from the **ptz** at the L_B site to the **ptzO** at either the L_A or L_B sites. The hypothesis was computationally rationalized by the relative highest energy occupied molecular orbital (HOMO) and lowest energy unoccupied molecular orbital (LUMO) energetic profiles of H_3**ptz** and H_3**ptzO**. As shown in Figure 6C, the computed orbital energies of the geometrically optimized ligands revealed that H_3**ptzO** has a larger HOMO-LUMO gap than H_3**ptz** does. The LUMO orbital of H_3**ptz** is higher in energy than that in H_3**ptzO**, meaning that it is possible for the photoexcited electron residing at the LUMO of H_3**ptz** to be readily transferred to the LUMO of H_3**ptzO**. This electron transfer event can take place in the framework under light irradiation[58] and theoretically lead to the generation of 3 kinds of radicals in the framework, 1 **ptz**$^{+\bullet}$ radical at the L_B site and 2 **ptzO**$^{-\bullet}$ radicals located at the L_A and L_B sites, respectively. These 3 radicals are expected to show varied redox potentials due to the differences in the chemical environment. To experimentally characterize these 3 radicals in the framework, we exploited the redox potential differences of the radical sites and titrated these radicals with ferrocenium (Fc^+) tetrafluoroborate. The titration of radical species in EPR studies has been reported as a technique in studying plasmonic nanocrystal properties.[59–61] To this end, a variety of radical trappers,[59–61] including Fc^+ tetrafluoroborate[62,63] have been reported. Fc^+ is a paramagnetic single electron reducing reagent that can quantitatively reduce and eliminate radicals in the material. We conducted an EPR measurement on PCN-401β at 4 K and observed 3 separate half-spin radicals (g values of 1.9550, 2.0001, and 2.0604) (Figure 6B). Then, an Fc^+ solution was titrated into the system while an EPR measurement was taken between each addition, tracking the existence and extinction of each radical (full experimental details are listed in the supplemental information and Figure S24). As shown in Figure 6B, the signals accounting for each of the radicals disappeared one by one rather than a uniform decrease across all of the signals. This indicates that the radicals are not coupled to one another and are indeed 3 separate half-spin radical signals. We therefore conclude that there are 3 different kinds of radicals in the β phase of PCN-401 corresponding to the 3 different ligand environments in the structure.

With all of the evidence obtained from the experimental data, a clear mechanism is proposed to show how the photoinduced phase transition is provoked and how the properties of PCN-401 are changed during the phase transition (Figure 6D). Upon UV irradiation, the **ptz** linkers located at the L_B site are excited and donate an electron to the **ptzO** linkers in proximity to the **ptz** within the framework. This electron transfer event induces the formation of **ptz**$^{+\bullet}$ and **ptzO**$^{-\bullet}$ radicals in the framework and subsequently causes the configuration shift in these linkers to adapt to the electronic structures. Synergistically, these configuration shifts lead to global structural transformation and eventually provoke the α-to-β phase transition. Although the β phase is not thermodynamically stable, the β-to-α transition is deterred kinetically by the global constrain from the framework. Such a kinetic barrier is positively correlated with the **ptz** content in the framework. This light-induced phase transition is accompanied by changes in a series of macroscopic properties as a result of the uniform and ordered structural transformation at a microscopic level. Upon phase transition, new absorption peaks arise and fluorescence disappears, both of which are caused by the electronic structural change. The anisotropic stiffening of the crystal is caused by a global structural transition that changes the pore environment and the subsequent O_2/CO_2 selectivity.

Phenothiazine as a photoresponsive unit possesses unique photochemical properties and light-induced isomerization behavior that promise a great potential in the construction of photoresponsive metal-organic materials. However, the research in the field of such materials featuring the uniqueness of phenothiazine had been

quite limited. This work serves as the first systematic investigation of a phenothiazine-based photoresponsive MOF, PCN-401. The rare *in situ* oxidation during the solvothermal synthesis of PCN-401 allowed for precise control over the crystallite formation with oxygen content. The crystal-to-crystal phase transition induced by light irradiation was structurally characterized by SCXRD studies. The pore environment and shape change during the light-induced transition significantly influence the gas sorption properties of the PCN-401. The uniform and synergistic atomic movements induced by light also result in anisotropic stiffening of the materials as evidenced by the nanoindentation experiments on different crystal faces. With systematic investigation, the mechanisms of the light-induced phase transition in PCN-401 were fully depicted by a series of experiments on the PCN-401 with varied amounts of **ptz**. The mechanisms proposed in this work can inspire future research on the phenothiazine-based metal organic materials. The phase transition triggered by a PIET mediated by **ptz** provides a rare example of the existence of stable radicals in the MOF structures. As a fundamental study, this work pushes the boundaries of our understanding of structure-property dynamic influences of photoresponsive frameworks under light irradiation and has implications for other dynamic systems.

EXPERIMENTAL PROCEDURES

Resource availability

Lead contact

Further information and requests should be directed to and will be fulfilled by the lead contact, Hong-Cai Zhou (zhou@chem.tamu.edu).

Materials availability

All of the materials generated in this study are available from the lead contact.

Data and code availability

Single crystal information may be obtained through the Cambridge Crystallographic Data Centre (CCDC) free of charge for structures with the deposition numbers of 2157065 (PCN-401α) and 2157078 (PCN-401β) and as Data S1 and S2.

Synthesis of PCN-401 single crystals

To a 4-mL vial we added $Zn(NO_3)_2 \cdot 6H_2O$ (100 mg) and high-performance liquid chromatography (HPLC)-grade *N*,*N*-dimethylformamide (DMF) (1.0 mL). The solution was dissolved via sonication. Once dissolved, concentrated HCl (14 μL) was added by pipette, followed by a solution of the H_3**ptz** ligand (10 mg solid in 2.0 mL HPLC-grade DMF). The clear solution was sealed in the vial and heated to 85°C for up to 9 days, yielding light mustard yellow crystals (yield = 8.5 mg). A longer crystallite formation typically resulted in a higher **ptz** ratio in the L_B as well as an improvement in crystalline quality. To wash the crystals, the solution must be decanted immediately while the solution is still hot and replaced with fresh HPLC-grade DMF.

L_B ligand ratio of ptz:ptzO variations of PCN-401

The synthesis of PCN-401 was performed using the same method as the single crystal synthesis of the MOF. A 20-mL portion of HPLC-grade DMF was oxygenated through strong ultrahigh purity (UHP) oxygen bubbling for 90 min (solution A). A second 20-mL portion of HPLC-grade DMF was degassed with strong UHP nitrogen bubbling for 90 min (solution B). The MOF samples were prepared with the following solvent ratios (A:B): 0:1, 1:3, 1:1, 3:1, and 1:0. The vials were sealed and heated at 80°C for 9 days. The crystallite formation time for the samples was as follows: 2 days (1:0), 4 days (3:1), 5 days (1:1), 7 days (1:3), 9 days (0:1). ^{1}H NMR ratios of

ptz/ptzO of the decomposed MOF products in D^6-DMSO and single crystals may be seen in Figures S3–S6 and S21.

SUPPLEMENTAL INFORMATION

Supplemental information can be found online at https://doi.org/10.1016/j.xcrp.2022.101074.

ACKNOWLEDGMENTS

H.F.D., G.S.D., and M.R.R. acknowledge the US Department of Energy (DOE) Office of Science Graduate Student Research (SCGSR) program for funding. The SCGSR program is administered by the Oak Ridge Institute for Science and Education (ORISE) for the DOE under contract no. DE-SC0014664. M.R.R. also acknowledges the US DOE Office of Science, Office of Basic Energy Sciences, Chemical Sciences, Geosciences, and Biosciences Division (Separation Sciences) for research funding and the National Energy Research Scientific Computing Center (NERSC), a DOE Office of Science User Facility operated under contract no. DE-AC02-05CH11231 for access to supercomputing resources. This work was produced by UT-Battelle LLC under Contract No. DE-AC05-00OR22725 with the US DOE. H.-C.Z. acknowledges the Robert A. Welch Foundation for a Welch Endowed Chair (A-0030) and the financial support of the Qatar National Research Fund award NPRP9-377-1-080. H.-C.Z. also acknowledges the Center for Gas Separations Relevant to Clean Energy Technologies, an Energy Frontier Research Center funded by the US DOE Office of Science (Basic Energy Sciences) under contract no. DE-SC0001015. In addition, the authors acknowledge the Texas A&M University (TAMU) X-ray Diffraction Laboratory and the NMR User Facility. The facilities of the Materials Characterization Facility (RRID: SCR_022202) at TAMU are acknowledged, and in particular, Dr. Wilson Serem is acknowledged for assistance with the nanoindentation studies. The TAMU Laboratory for Biological Mass Spectrometry (LBMS) facility and Dr. Yohannes Rezenom are gratefully acknowledged. This research used resources at the Advanced Light Source at Lawrence Berkeley National Laboratory (LBNL), a DOE Office of Science User Facility operated under contract no. DE-AC02-05CH11231 by LBNL. Beamline 12.2.1 and Dr. Simon J. Teat (LBNL) are gratefully acknowledged. The manuscript is funded by the Welch Foundation for a Welch Endowed Chair (A-0030), the Qatar National Research Fund (NPRP9-377-1-080), the Oak Ridge Institute for Science and Education (DE-SC0014664), and Basic Energy Sciences (DE-SC0001015).

AUTHOR CONTRIBUTIONS

Conceptualization, M.R.R., H.-C.Z., H.F.D., and Z.X.; methodology, H.F.D. and Z.X.; investigation, H.F.D. and Z.X.; materials generation, H.F.D. and H.L.; BET measurements, H.F.D.; spectroscopic measurements, H.F.D., Z.X., and H.L.; EPR data measurement and analyses, H.F.D., J.E.K., and H.X.; theoretical calculations, P.C.; draft writing and editing, Z.X., H.F.D., and G.S.D.; funding acquisition, M.R.R. and H.-C.Z.; all of the authors discussed the data and contributed to the paper.

DECLARATION OF INTERESTS

The authors declare no competing interests.

Received: August 2, 2022
Revised: September 8, 2022
Accepted: September 9, 2022
Published: September 29, 2022

REFERENCES

1. Rice, A.M., Martin, C.R., Galitskiy, V.A., Berseneva, A.A., Leith, G.A., and Shustova, N.B. (2020). Photophysics modulation in photoswitchable metal–organic frameworks. Chem. Rev. *120*, 8790–8813. https://doi.org/10.1021/acs.chemrev.9b00350.

2. Liu, Z., Zhang, L., and Sun, D. (2020). Stimuli-responsive structural changes in metal–organic frameworks. Chem. Commun. *56*, 9416–9432. https://doi.org/10.1039/D0CC03197F.

3. Drake, H.F., Day, G.S., Xiao, Z., Zhou, H.-C., and Ryder, M.R. (2022). Light-induced switchable adsorption in azobenzene- and stilbene-based porous materials. Trends Chem. *4*, 32–47. https://doi.org/10.1016/j.trechm.2021.11.003.

4. Danowski, W., van Leeuwen, T., Browne, W.R., and Feringa, B.L. (2021). Photoresponsive porous materials. Nanoscale Adv. *3*, 24–40. https://doi.org/10.1039/D0NA00647E.

5. Park, J., Feng, D., Yuan, S., and Zhou, H.-C. (2015). Photochromic metal–organic frameworks: reversible control of singlet oxygen generation. Angew. Chem. Int. Ed. Engl. *54*, 430–435. https://doi.org/10.1002/anie.201408862.

6. Mondal, B., Ghosh, A.K., and Mukherjee, P.S. (2017). Reversible multistimuli switching of a spiropyran-functionalized organic cage in solid and solution. J. Org. Chem. *82*, 7783–7790. https://doi.org/10.1021/acs.joc.7b00722.

7. Dolgopolova, E.A., Ejegbavwo, O.A., Martin, C.R., Smith, M.D., Setyawan, W., Karakalos, S.G., Henager, C.H., zur Loye, H.-C., and Shustova, N.B. (2017). Multifaceted modularity: a key for stepwise building of hierarchical complexity in actinide metal–organic frameworks. J. Am. Chem. Soc. *139*, 16852–16861. https://doi.org/10.1021/jacs.7b09496.

8. Dolgopolova, E.A., Galitskiy, V.A., Martin, C.R., Gregory, H.N., Yarbrough, B.J., Rice, A.M., Berseneva, A.A., Ejegbavwo, O.A., Stephenson, K.S., Kittikhunnatham, P., et al. (2019). Connecting wires: photoinduced electronic structure modulation in metal–organic frameworks. J. Am. Chem. Soc. *141*, 5350–5358. https://doi.org/10.1021/jacs.8b13853.

9. Dolgopolova, E.A., Moore, T.M., Ejegbavwo, O.A., Pellechia, P.J., Smith, M.D., and Shustova, N.B. (2017). A metal–organic framework as a flask: photophysics of confined chromophores with a benzylidene imidazolinone core. Chem. Commun. *53*, 7361–7364. https://doi.org/10.1039/C7CC02253K.

10. Williams, D.E., Martin, C.R., Dolgopolova, E.A., Swifton, A., Godfrey, D.C., Ejegbavwo, O.A., Pellechia, P.J., Smith, M.D., and Shustova, N.B. (2018). Flipping the switch: fast photoisomerization in a confined environment. J. Am. Chem. Soc. *140*, 7611–7622. https://doi.org/10.1021/jacs.8b02994.

11. Kim, M., Cahill, J.F., Su, Y., Prather, K.A., and Cohen, S.M. (2012). Postsynthetic ligand exchange as a route to functionalization of metal-organic frameworks. Chem. Sci. *3*, 126–130. https://doi.org/10.1039/C1SC00394A.

12. Li, H., Martinez, M.R., Perry, Z., Zhou, H.-C., Falcaro, P., Doblin, C., Lim, S., Hill, A.J., Halstead, B., and Hill, M.R. (2016). A robust metal-organic framework for dynamic light-induced swing adsorption of Carbon dioxide. Chemistry *22*, 11176–11179. https://doi.org/10.1002/chem.201602671.

13. Li, H., Sadiq, M.M., Suzuki, K., Doblin, C., Lim, S., Falcaro, P., Hill, A.J., and Hill, M.R. (2016). MaLISA - a cooperative method to release adsorbed gases from metal-organic frameworks. J. Mater. Chem. *4*, 18757–18762. https://doi.org/10.1039/C6TA09826F.

14. Li, H., Sadiq, M.M., Suzuki, K., Ricco, R., Doblin, C., Hill, A.J., Lim, S., Falcaro, P., and Hill, M.R. (2016). Magnetic metal-organic frameworks for efficient Carbon dioxide capture and remote trigger release. Adv. Mater. *28*, 1839–1844. https://doi.org/10.1002/adma.201505320.

15. Li, Z., Wang, G., Ye, Y., Li, B., Li, H., and Chen, B. (2019). Loading photochromic molecules into a luminescent metal–organic framework for information anticounterfeiting. Angew. Chem. Int. Ed. Engl. *58*, 18025–18031. https://doi.org/10.1002/anie.201910467.

16. Müller, K., Wadhwa, J., Singh Malhi, J., Schöttner, L., Welle, A., Schwartz, H., Hermann, D., Ruschewitz, U., and Heinke, L. (2017). Photoswitchable nanoporous films by loading azobenzene in metal-organic frameworks of type HKUST-1. Chem. Commun. *53*, 8070–8073. https://doi.org/10.1039/C7CC00961E.

17. Garg, S., Schwartz, H., Kozlowska, M., Kanj, A.B., Müller, K., Wenzel, W., Ruschewitz, U., and Heinke, L. (2019). Conductance photoswitching of metal–organic frameworks with embedded spiropyran. Angew. Chem. Int. Ed. Engl. *58*, 1193–1197. https://doi.org/10.1002/anie.201811458.

18. Heinke, L., Cakici, M., Dommaschk, M., Grosjean, S., Herges, R., Bräse, S., and Wöll, C. (2014). Photoswitching in two-component surface-mounted metal–organic frameworks: optically triggered release from a molecular container. ACS Nano *8*, 1463–1467. https://doi.org/10.1021/nn405469g.

19. Kanj, A.B., Bürck, J., Grosjean, S., Bräse, S., and Heinke, L. (2019). Switching the enantioselectivity of nanoporous host materials by light. Chem. Commun. *55*, 8776–8779. https://doi.org/10.1039/C9CC02849H.

20. Müller, K., Knebel, A., Zhao, F., Bléger, D., Caro, J., and Heinke, L. (2017). Switching thin films of azobenzene-containing metal–organic frameworks with visible light. Chemistry *23*, 5434–5438. https://doi.org/10.1002/chem.201700989.

21. Schwartz, H.A., Ruschewitz, U., and Heinke, L. (2018). Smart nanoporous metal–organic frameworks by embedding photochromic molecules – state of the art and future perspectives. Photochem. Photobiol. Sci. *17*, 864–873. https://doi.org/10.1039/C7PP00456G.

22. Wang, Z., Müller, K., Valášek, M., Grosjean, S., Bräse, S., Wöll, C., Mayor, M., and Heinke, L. (2018). Series of photoswitchable azobenzene-containing metal–organic frameworks with variable adsorption switching effect. J. Phys. Chem. C *122*, 19044–19050. https://doi.org/10.1021/acs.jpcc.8b05843.

23. Lo, S.-H., Feng, L., Tan, K., Huang, Z., Yuan, S., Wang, K.-Y., Li, B.-H., Liu, W.-L., Day, G.S., Tao, S., et al. (2020). Rapid desolvation-triggered domino lattice rearrangement in a metal–organic framework. Nat. Chem. *12*, 90–97. https://doi.org/10.1038/s41557-019-0364-0.

24. Zheng, Y., Sato, H., Wu, P., Jeon, H.J., Matsuda, R., and Kitagawa, S. (2017). Flexible interlocked porous frameworks allow quantitative photoisomerization in a crystalline solid. Nat. Commun. *8*, 100. https://doi.org/10.1038/s41467-017-00122-5.

25. Chen, X., Xie, H., Lorenzo, E.R., Zeman, C.J., Qi, Y., Syed, Z.H., Stone, A.E.B.S., Wang, Y., Goswami, S., Li, P., et al. (2022). Direct observation of modulated radical spin states in metal–organic frameworks by controlled flexibility. J. Am. Chem. Soc. *144*, 2685–2693. https://doi.org/10.1021/jacs.1c11417.

26. Sun, D., Rosokha, S.V., and Kochi, J.K. (2004). Donor-acceptor (electronic) coupling in the precursor complex to organic electron transfer: intermolecular and intramolecular self-exchange between phenothiazine redox centers. J. Am. Chem. Soc. *126*, 1388–1401. https://doi.org/10.1021/ja038746v.

27. Ronzani, F., Trivella, A., Arzoumanian, E., Blanc, S., Sarakha, M., Richard, C., Oliveros, E., and Lacombe, S. (2013). Comparison of the photophysical properties of three phenothiazine derivatives: transient detection and singlet oxygen production. Photochem. Photobiol. Sci. *12*, 2160–2169. https://doi.org/10.1039/c3pp50246e.

28. Christensen, J.A., Phelan, B.T., Chaudhuri, S., Acharya, A., Batista, V.S., and Wasielewski, M.R. (2018). Phenothiazine radical cation excited states as super-oxidants for energy-demanding reactions. J. Am. Chem. Soc. *140*, 5290–5299. https://doi.org/10.1021/jacs.8b01778.

29. Freitas, V.L., Gomes, J.R., and Ribeiro da Silva, M.D. (2014). Structural, energetic and reactivity properties of phenoxazine and phenothiazine. J. Chem. Therm. *73*, 110–120. https://doi.org/10.1016/j.jct.2013.11.013.

30. Fang, Y., Lian, X., Huang, Y., Fu, G., Xiao, Z., Wang, Q., Nan, B., Pellois, J.P., and Zhou, H.C. (2018). Investigating subcellular compartment targeting effect of porous coordination cages for enhancing cancer nanotherapy. Small *14*, e1802709. https://doi.org/10.1002/smll.201802709.

31. Franz, A.W., Rominger, F., and Müller, T.J.J. (2008). Synthesis and electronic properties of sterically demanding N-arylphenothiazines and unexpected buchwald-Hartwig aminations. J. Org. Chem. *73*, 1795–1802. https://doi.org/10.1021/jo702389v.

32. Rupérez, F., Conesa, J.C., and Soria, J. (1984). EPR study of the phenothiazine cation radical. Spectrochim. Acta Mol. Spectros *40*, 1021–1024. https://doi.org/10.1016/0584-8539(84)80129-4.

33. Bodea, C., and Silberg, I. (1968). Recent advances in the chemistry of phenothiazines. Adv. Heterocycl. Chem. *9*, 321–460. https://doi.org/10.1016/s0065-2725(08)60375-x.

34. Beckett, A.H., and Navas, G.E. (1978). Aromatic oxidation of some phenothiazines. Xenobiotica *8*, 721–736. https://doi.org/10.3109/00498257809069585.

35. Abdallah, M., Bui, T.-T., Goubard, F., Theodosopoulou, D., Dumur, F., Hijazi, A., Fouassier, J.-P., and Lalevée, J. (2019). Phenothiazine derivatives as photoredox catalysts for cationic and radical photosensitive resins for 3D printing technology and photocomposite synthesis. Polym. Chem. *10*, 6145–6156. https://doi.org/10.1039/c9py01265f.

36. Gu, C., Hosono, N., Zheng, J.-J., Sato, Y., Kusaka, S., Sakaki, S., and Kitagawa, S. (2019). Design and control of gas diffusion process in a nanoporous soft crystal. Science *363*, 387–391. https://doi.org/10.1126/science.aar6833.

37. Quddus, E.B., Wilson, A., Webb, R.A., and Koley, G. (2014). Oxygen mediated synthesis of high quality InN nanowires above their decomposition temperature. Nanoscale *6*, 1166–1172. https://doi.org/10.1039/C3NR03991A.

38. Blatov, V.A., Shevchenko, A.P., and Proserpio, D.M. (2014). Applied topological analysis of crystal structures with the program package ToposPro. Cryst. Growth Des. *14*, 3576–3586. https://doi.org/10.1021/cg500498k.

39. Nelson, A.P., Farha, O.K., Mulfort, K.L., and Hupp, J.T. (2009). Supercritical processing as a route to high internal surface areas and permanent microporosity in Metal−Organic framework materials. J. Am. Chem. Soc. *131*, 458–460. https://doi.org/10.1021/ja808853q.

40. Kaur, J., and Kaur, G. (2021). Review on flexible metal-organic frameworks. ChemistrySelect *6*, 8227–8243. https://doi.org/10.1002/slct.202101524.

41. Thommes, M., Kaneko, K., Neimark, A.V., Olivier, J.P., Rodriguez-Reinoso, F., Rouquerol, J., and Sing, K.S. (2015). Physisorption of gases, with special reference to the evaluation of surface area and pore size distribution (IUPAC Technical Report). Pure Appl. Chem. *87*, 1051–1069. https://doi.org/10.1515/pac-2014-1117.

42. Drake, H.F., Xiao, Z., Day, G.S., Vali, S.W., Daemen, L.L., Cheng, Y., Cai, P., Kuszynski, J.E., Lin, H., Zhou, H.-C., and Ryder, M.R. (2022). Influence of metal identity on light-induced switchable adsorption in azobenzene-based metal–organic frameworks. ACS Appl. Mater. Interfaces *14*, 11192–11199. https://doi.org/10.1021/acsami.1c18266.

43. Kamat, P.V., and Lichtin, N.N. (1981). Photoinduced electron-ejection from methylene blue in water and acetonitrile. J. Phys. Chem. *85*, 3864–3868. https://doi.org/10.1021/j150625a031.

44. Kayser, R.H., and Young, R.H. (1976). The photoreduction of methylene blue by amines I. a flash photolysis study of the reaction between triplet methylene blue and amines. Photochem. Photobiol. *24*, 395–401. https://doi.org/10.1111/j.1751-1097.1976.tb06845.x.

45. Shine, H.J., and Mach, E.E. (1965). Ion radicals. V. Phenothiazine, phenothiazine 5-oxide, and phenothiazone-3 in acid Solutions1, 2. J. Org. Chem. *30*, 2130–2139. https://doi.org/10.1021/jo01018a004.

46. Spek, A.L. (2015). PLATON SQUEEZE: a tool for the calculation of the disordered solvent contribution to the calculated structure factors. Acta Crystallogr. C Struct. Chem. *71*, 9–18. https://doi.org/10.1107/S2053229614024929.

47. Yao, Z.-S., Mito, M., Kamachi, T., Shiota, Y., Yoshizawa, K., Azuma, N., Miyazaki, Y., Takahashi, K., Zhang, K., Nakanishi, T., et al. (2014). Molecular motor-driven abrupt anisotropic shape change in a single crystal of a Ni complex. Nat. Chem. *6*, 1079–1083. https://doi.org/10.1038/nchem.2092.

48. Naumov, P., Chizhik, S., Panda, M.K., Nath, N.K., and Boldyreva, E. (2015). Mechanically responsive molecular crystals. Chem. Rev. *115*, 12440–12490. https://doi.org/10.1021/acs.chemrev.5b00398.

49. Tricarico, M., and Tan, J.-C. (2022). Mechanical properties and nanostructure of monolithic zeolitic imidazolate frameworks: a nanoindentation, nanospectroscopy and finite-element study. Mater. Today Nano *17*, 100166. https://doi.org/10.1016/j.mtnano.2021.100166.

50. Burtch, N.C., Heinen, J., Bennett, T.D., Dubbeldam, D., and Allendorf, M.D. (2018). Mechanical properties in metal–organic frameworks: emerging opportunities and challenges for device functionality and technological applications. Adv. Mater. *30*, 1704124. https://doi.org/10.1002/adma.201704124.

51. Redfern, L.R., and Farha, O.K. (2019). Mechanical properties of metal–organic frameworks. Chem. Sci. *10*, 10666–10679. https://doi.org/10.1039/C9SC04249K.

52. Drake, H.F., Xiao, Z., Day, G.S., Vali, S.W., Chen, W., Wang, Q., Huang, Y., Yan, T.-H., Kuszynski, J.E., Lindahl, P.A., et al. (2021). Thermal decarboxylation for the generation of hierarchical porosity in isostructural metal–organic frameworks containing open metal sites. Mater. Adv. *2*, 5487–5493. https://doi.org/10.1039/D1MA00163A.

53. Campillo-Alvarado, G., D'Mello, K.P., Swenson, D.C., Santhana Mariappan, S.V., Höpfl, H., Morales-Rojas, H., and MacGillivray, L.R. (2019). Exploiting boron coordination: B←N bond supports a [2+2] photodimerization in the solid state and generation of a diboron bis-tweezer for benzene/thiophene separation. Angew. Chem. Int. Ed. Engl. *58*, 5413–5416. https://doi.org/10.1002/anie.201812174.

54. Moreno-Piraján, J.C., and Giraldo, L. (2020). Heat of adsorption: a comparative study between the experimental determination and theoretical models using the system CH4-MOFs. J. Chem. Eng. Data *65*, 3130–3145. https://doi.org/10.1021/acs.jced.0c00159.

55. Langmuir, I. (1918). The adsorption of gases on plane surfaces of glass, mica and platinum. J. Am. Chem. Soc. *40*, 1361–1403. https://doi.org/10.1021/ja02242a004.

56. Cai, L.-Z., Yao, Z.-Z., Lin, S.-J., Wang, M.-S., and Guo, G.-C. (2021). Photoinduced electron-transfer (PIET) strategy for selective adsorption of CO2 over C2H2 in a MOF. Angew. Chem. Int. Ed. Engl. *60*, 18223–18230. https://doi.org/10.1002/anie.202105491.

57. Vázquez, A., Tudela, J., Varón, R., and García-Cánovas, F. (1992). Determination of the molar absorptivities of phenothiazine cation radicals generated by oxidation with hydrogen peroxide/peroxidase. Anal. Biochem. *202*, 245–248. https://doi.org/10.1016/0003-2697(92)90101-C.

58. Martin, C.R., Park, K.C., Leith, G.A., Yu, J., Mathur, A., Wilson, G.R., Gange, G.B., Barth, E.L., Ly, R.T., Manley, O.M., et al. (2022). Stimuli-modulated metal oxidation states in photochromic MOFs. J. Am. Chem. Soc. *144*, 4457–4468. https://doi.org/10.1021/jacs.1c11984.

59. Conti, C.R., McBride, J.R., and Strouse, G.F. (2021). Examining the effect of dopant ionic radius on plasmonic M:ZnO nanocrystals (M = Al3+, Ga3+, In3+). J. Phys. Chem. C *125*, 7772–7779. https://doi.org/10.1021/acs.jpcc.1c00529.

60. Conti, C.R., III, Quiroz-Delfi, G., Schwarck, J.S., Chen, B., and Strouse, G.F. (2020). Carrier density, effective mass, and nuclear relaxation pathways in plasmonic Sn:In2O3 nanocrystals. J. Phys. Chem. C *124*, 28220–28229. https://doi.org/10.1021/acs.jpcc.0c09448.

61. Kays, J.C., Conti, C.R., Margaronis, A., Kuszynski, J.E., Strouse, G.F., and Dennis, A.M. (2021). Controlled synthesis and exploration of CuxFeS4 bornite nanocrystals. Chem. Mater. *33*, 7408–7416. https://doi.org/10.1021/acs.chemmater.1c02029.

62. Connelly, N.G., and Geiger, W.E. (1996). Chemical redox agents for organometallic chemistry. Chem. Rev. *96*, 877–910. https://doi.org/10.1021/cr940053x.

63. Araujo, J.J., Brozek, C.K., Liu, H., Merkulova, A., Li, X., and Gamelin, D.R. (2021). Tunable band-edge potentials and charge storage in colloidal tin-doped indium oxide (ITO) nanocrystals. ACS Nano *15*, 14116–14124. https://doi.org/10.1021/acsnano.1c04660.